ELSEVIER

Journal of Nuclear Materials 290–293 (2001) 402–406

journal of nuclear materials

www.elsevier.nl/locate/jnucmat

Particle trapping in carbon walls during ICRH heating in Tore Supra

C. Grisolia [a,*], J. Hogan [b], Ph. Ghendrih [a], Th. Loarer [a], J. Gunn [a], P. Monier-Garbet [a], M. Becoulet [a], Th. Hutter [a]

[a] *Association Euratom-CEA, DRFC, CE A Cadarache, 13108 St-Paul-lez-Durance, France*
[b] *Fusion Energy Division, Oak Ridge National Laboratory, Oak Ridge, TN 37830, USA*

Abstract

The role of high-energy charge exchange (CX) particles during radio-frequency (RF) heating is examined in an attempt to develop a predictive model for wall saturation and desaturation processes. Tore Supra discharges in which an apparent saturated wall, previously obtained through a succession of ohmic discharges, was transformed into a pumping wall with the application of RF heating are analyzed. Direct measurements show the increased mean energy of the CX spectrum upon application of RF heating. This leads to deeper CX neutrals penetration reaching the remaining a:C–D unsaturated layer and restoring the wall pumping efficiency. The conversion from a saturated to a pumping state with the application of RF heating, and the time scales for saturation during the ohmic and the heating phases, are reasonably well explained by several existing models. The deeper particle wall penetration observed during RF plasma experiments points to a potential mechanism which can increase tritium trapping in a fusion reactor.

Keywords: Hydrogen trapping; Tore Supra

1. Introduction

Plasma wall particle exchange in graphite-armored fusion devices plays a crucial role in tritium retention in present (JET or TFTR) or in future experiments (such as ITER).

Plasma wall particle exchange in a discharge involves both direct recycling from the plasma-facing surfaces and the charge exchange (CX) efflux [1–3] which has a similar magnitude. High-energy CX particles can penetrate deeply into the wall, reach a previously unsaturated layer (if pre-existing), and thus be trapped for a longer time leading to effective wall pumping efficiency. The importance of these particles produced during ICRH heating will be examined in order to better understand wall saturation and desaturation processes. RF heating experiments are especially useful here since the neutral beam fueling and accompanying 'halo' CX flux are absent.

Several wall models exist which combine rates for post-discharge wall equilibration with semi-empirical rates for plasma-induced particle exchange with a:C–D surfaces. The testing of several of these models with additional heating is pursued in this paper. These are referred to subsequently as the JET DTE1 [4], the PTE [5] and the Tore Supra [6] models. Previous work [5,6] has led to the formulation of estimates for basic trapping, de-trapping and recombination rates. Particle-induced desorption (P-ID) has been studied and a semi-empirical value for the P-ID rate was tested for ohmic conditions [4], following the model of [7].

Deuterium retention capacity in a:C–D layer varies as a function of deuterium content [8]. Retention capability increases for 'soft' films to almost 100% of the carbon density, larger than the ~40% value commonly assumed. Further, as the deuterium content of the a:C–D film increases, the effective range of energetic

* Corresponding author. Tel.: +33-4 42 25 43 78; fax: +33-4 42 25 49 90.
E-mail address: grisolia@drfc.cad.cea.fr (C. Grisolia).

0022-3115/01/$ - see front matter
PII: S0022-3115(00)00509-2

particles is increased. Thus previous models must reflect these properties.

In the following, the degree to which some present wall models exhibit the observed transition from saturated to pumping behavior when additional heating is applied will be tested.

2. Discharges with additional (RF) heating

After boronization, Tore Supra discharge series began with wall loading ohmic discharges. Here, the Tore Supra ergodic divertor (ED) was used in order to decrease the plasma edge temperature (down to 25 eV) and to saturate the walls more rapidly. Two ED shots and 19 Pa m^3 of injected deuterium were required. During a following ohmic shot (without ED) a detached plasma was obtained without gas injection, which confirms wall saturation (see Fig. 1(a)).

Following ohmic saturation, a series of discharges was made, without the ED but with ICRH power varying from 3.8 to 9 MW. The plasma was limited by the outboard pump limiter and was far from the inner wall (~11 cm). Plasma density decreases indicating that the wall had returned to a pumping state in spite of its prior saturation (Fig. 1(b)). Moreover, the gas injection needed to reach the same plasma density in the ohmic phase (just before ICRH) increases from 1.5 Pa m^3 during the first shot to 4 Pa m^3 in the third indicating again wall desaturation. It should also be noted that there is an increase of density observed when ICRH is turned on for each shot, and this should be explained by the model.

The measured energetic CX flux changes with applied RF power (see Fig. 2).The CX flux ($E > 1$ keV) is relatively low during the OH sequence (26 794, Fig. 2(a)) but increases sharply during RF heating (26 798, Fig. 2(a)). These flux measurements directly indicate the orders of magnitude increase in the energetic component of the particle efflux produced by heating, relative to the thermal background. The edge ion temperature (deduced from CX) increases as expected with ICR heating. (Fig. 2(b) showing the OH and RF shots of Fig. 2(a)). The energy distribution is 'hardened', that is the mean energy is higher, leading to deeper CX flux penetration into the a:C–D layer.

Approach to wall saturation depends on the prior degree of wall saturation near the region where the ion recycling flux lands and where the CX flux is highest. In this experiment, saturating discharges were carried out using the ED, while the subsequent heating discharges were mainly resting on the outboard limiter. The implantation areas involved in both experiments are not the same and this must be taken into account in the analysis.

3. Modeling

Implantation areas are estimated using a 3-D Monte Carlo code for the transport of neutral deuterium

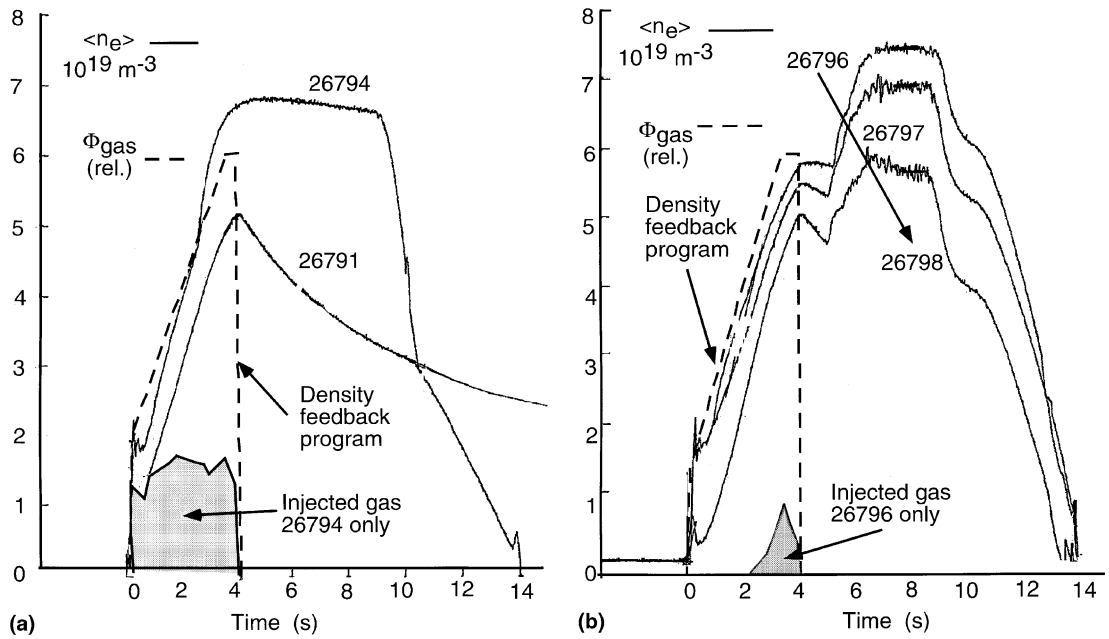

Fig. 1. (a) Density behavior during the ohmic saturation phase. (b) Density behavior during the first discharges with RF heating, with a previously saturated wall.

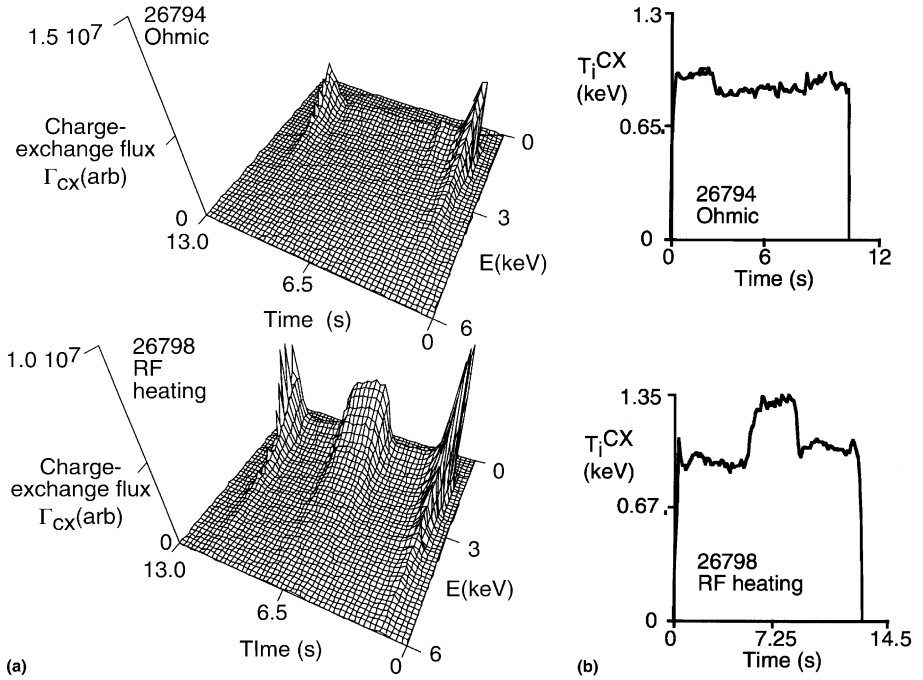

Fig. 2. (a) Time dependence of measured energy distribution of energetic ($E > 1$ keV) CX flux, $(G(E), t)$ for ohmic and RF-heated discharges. (b) Time dependence of edge T_i inferred from CX measurement for ohmic and RF heated discharges.

(D, D_2). A detailed simulation of the recycling and neutral transport both with the ED (loading phase) and the outboard limiter (heating phase) has been developed. The neutral transport model includes the relevant deuterium atomic and surface physics (Franck–Condon dissociation of D_2 and ionization and CX processes for D) and treats the real geometry of both the ED and the limiter [9]. For the ohmic phase bounded by the ED interacting surfaces, the D_2 density is found to be strongly localized near the ED face plates (Fig. 3(a)). These plates have a total surface area $\sim$6 m^2, 1/2 that of the inner wall. The D_0 density is peaked just inside the limiter surface (Fig. 3(b)). For the heating phase (plasma on the limiter), D_2 is strongly localized just outside the last closed flux surface (Fig. 3(b)) (active surface area $\sim$ 1 m^2) whereas D_0 density is just inside. During heating, mean energy of the CX particles closed to the limiter increases due to the increased sheath energy of the ion flux, and the increased value of T_i throughout the edge region from 25 eV (ED phase) to 150 eV (limiter phase).

The time-dependent evolution of the implantation is modeled with the SPUDNUT 1-D (flux surface averaged) neutral transport code which calculates the CX energy spectrum and thus, from TRIM range estimates [10], the depth distribution of the deposited CX efflux spectrum in the a:C–D layer. The deposition model has two parts: first the fraction of directly reflected particles is calculated, using the TRIM-code fast particle reflection model [10]. The remaining flux to the wall is then deposited according to the effective range estimates in [8] for 'hard' and 'soft' a-C:D films. For lower deuterium concentration in graphite (hard films), the effective range of CX particles will be reduced compared to the later stages of saturation (soft films) in which the effective deposition range increases [8]. Fig. 4 shows a comparison of the total accumulated deposition in the wall for discharges 26 794, −97 and −98, as calculated by the 1-D neutrals model using measured plasma profiles. Three cases are shown: hard (no D), 'nominal' (40% D, $R = 1.5$) and soft (80% D, $R = 2.0$) films, where R is the ratio of the effective range relative to the value for 'nominal' case. The deposition range (and the size of the effective unsaturated reservoir) is increased with the increase in deuterium concentration.

A model for hydrogen inventory dynamics in the surface is incorporated in the 1-D WDIFFUSE code [1–4]. WDIFFUSE calculates the evolution of D_2, following the space- and time-dependent evolution of both trapped (t) and solute (s) deuterium under the interaction of implanted fluxes. The net D_0 fluxes to the surface are the implantation driving terms which determine the changes in wall composition and hence in recycling coefficient. In the analysis we will assume that the properties of deuterium in the boronized layer are similar to those in an a:C–D layer, based on the analysis of laboratory experiments described in [11].

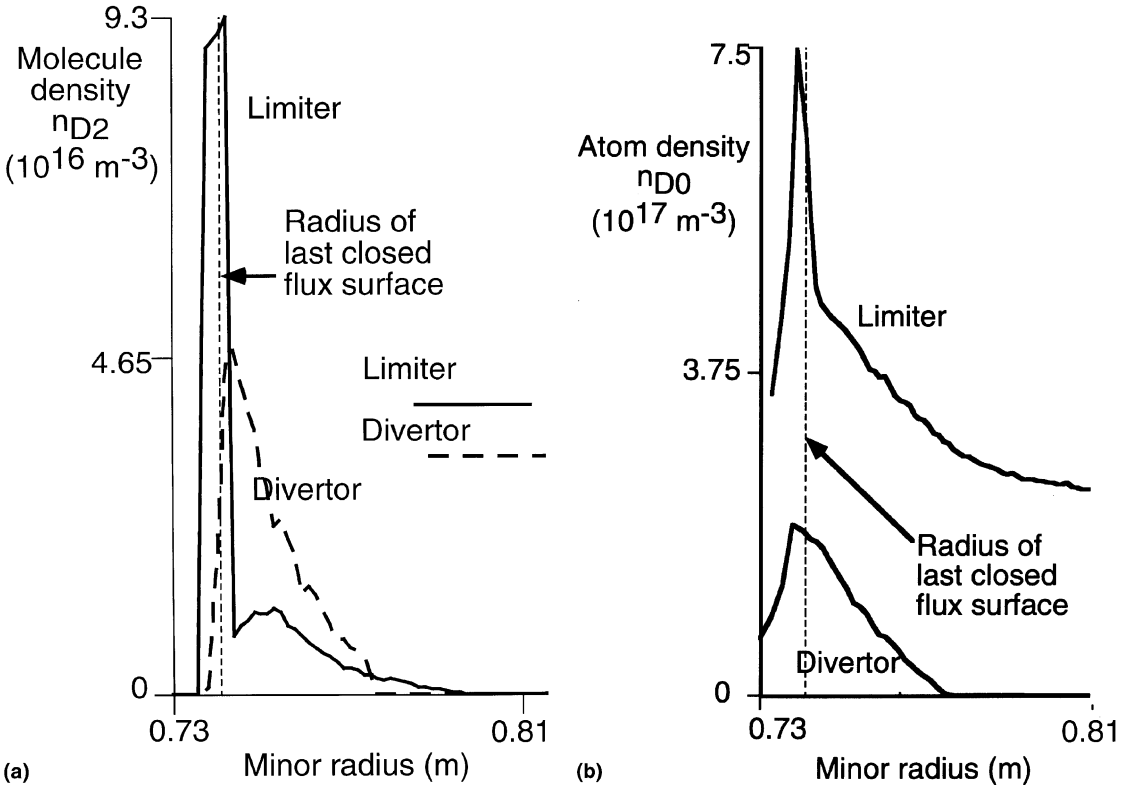

Fig. 3. Monte Carlo results for neutral D_0, D_2 radial distributions for ohmic phase (with divertor) and RF heating phase (limiter) (a) molecules, (b) atoms.

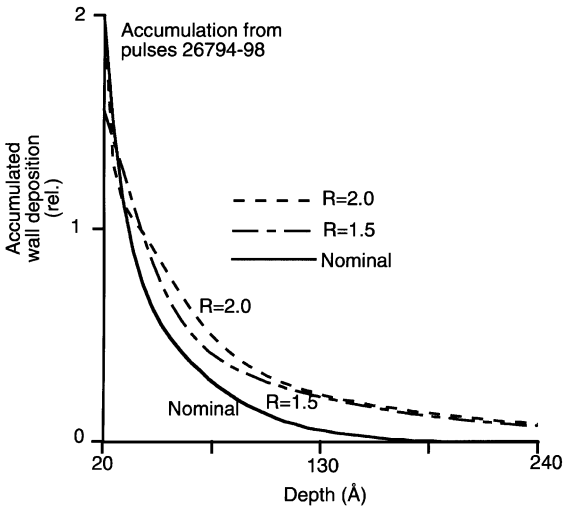

Fig. 4. Total deposition profiles for discharges 26 794, –97 and –98 for different assumptions about retention capability of increasingly soft films.

Wall model equations are presented elsewhere [4] with all the parameters of interest. Here diffusion processes are neglected since short shots are analyzed. This is not completely correct during ED saturation experiments since the particle deposition depth is small due to low ion temperature at the plasma edge. And finally, diffusion must be taken into account after shot outgassing and especially during long-pulse operation as in next step devices.

4. Evolution of wall saturation

Various models have been applied to ohmic saturation phase and heating conditions. The direct exchange surface area in the ohmic phase (~6 m^2) is higher than for the heating phase (~1 m^2). However, simple considerations show that this direct area cannot be the only interacting surface which has to be taken into account. Indeed with ohmic plasma parameters or in the heating case, it can be shown that with the above interacting area, saturation is reached in less than one second in both cases. Thus, only the total vacuum vessel area can serve as a sufficiently large reservoir to produce pumping with the onset of heating. The CX mechanism is well suited to use the whole vacuum vessel area, since the CX particles illuminate the whole region.

Thus, the response of the a:C–D films on the vacuum vessel wall area has been simulated using all the wall

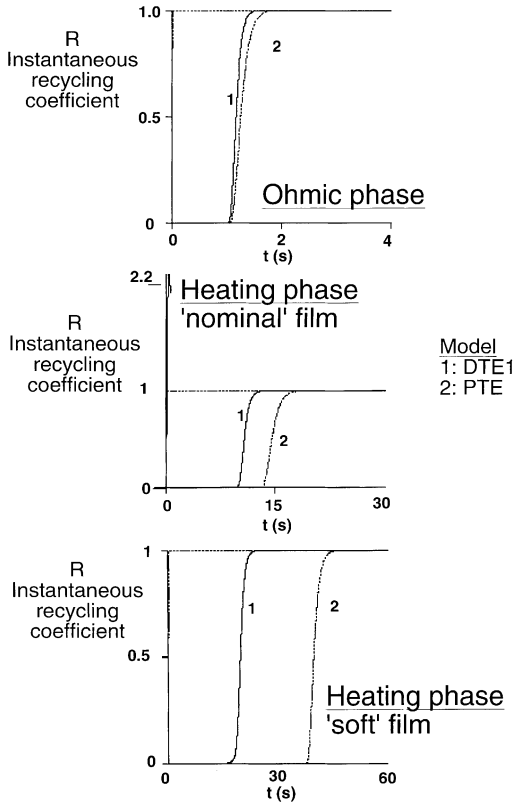

Fig. 5. Calculated response of wall diffusion models in the (a) ohmic saturation phase, (b) RF heating (pumping) phase.

models. Fig. 5(a) shows the response to the case which simulates the ohmic conditions (edge $T_i = 25$ eV) and Fig. 5(b) for the heating conditions (edge $T_i = 150$ eV). The recycling coefficient in the ohmic case reaches unity quickly and saturation is reached. The energetic CX flux in the heating case deposits new particles in a previously unsaturated area, so that there is no recycling of this flux. In this case, 15 s is required with the DTE1 and PTE models to return to a recycling condition.

If a soft film is assumed which leads to an increased deuterium capacity, the time required for onset of recycling increases proportionately for the models and becomes equal to 30 s.

5. Conclusions

The DTE1 and PTE models predict a similar (i.e., pumping) response to an energetic CX efflux due to the onset of RF heating. This energetic CX flux is deposited in a previously unsaturated region of the wall, and thus is not immediately recycled. In contrast, fluxes deposited in the region previously saturated during the lower-energy ohmic phase are recycled, and a continuing detached phase would be expected under these circumstances. Thus, the energetic CX model suggests a physically reasonable mechanism for an otherwise puzzling change in the recycling characteristics of the wall.

The instantaneous rise in density with the application of RF power in all the heating cases is a consequence of the increase in the total flux, of both high- and low-energy particles. Because the shallowest layers are always saturated, the increased efflux leads to an increased recycled flux and thus to higher density. However the more energetic particles are not recycled, and this produced pumping.

It is obvious, both from the wide range in values of the fundamental wall coefficients, as well as the lack of a direct quantitative characterization of the hard/soft nature of the a:C–D films, that this model agreement is qualitative at best and that more wall characterizing diagnostics are needed. Even so, this means that several models are candidates to predict the transition and so can be further explored to attain the goal of a predictive model. The present results also show that the dependence of the wall state on heating should be taken into account in the design for future burning plasmas, first of all to be able to attain the scenario which is needed for high-plasma confinement performance, but also to determine the source terms for coupling to possible diffusion of tritium into the bulk.

References

[1] J. Hogan, P. Mioduszewski, L. Owen et al., J. Nucl. Mater. 196–198 (1992) 1083.
[2] P. Mioduszewski, J. Hogan, L. Owen et al., J. Nucl. Mater. 220 (1995) 91.
[3] J. Hogan, R. Maingi, P. Mioduszewski et al., J. Nucl. Mater. 241 (1997) 612.
[4] D. Hillis, J. Hogan, P. Andrew et al., Phys. Plasmas 6 (1999) 1985.
[5] P. Andrew, P. Coad, J. Ehrenberg et al., Nucl. Fus. 33 (1993) 1389.
[6] C. Grisolia, L. Horton, J. Ehrenberg, J. Nucl. Mater. 220 (1995) 516.
[7] W. Moeller, B. Scherzer, J. Appl. Phys. 64 (1988) 4860.
[8] W. Jacob, Thin Solid Films 326 (1998) 1.
[9] S.J. Tobin, C. DeMichelis, J. Hogan et al., Plasma Phys. Cont. Fusion 40 (1998) 1335.
[10] W. Eckstein, IPP Report 9/117, Garching, 1998.
[11] K. Tsuzuki, K. Inoue, A. Sagara et al., NIFS Report, NIFS-500 Dynamic behavior of hydrogen atoms with a boronized wall, July 1997.